Linear Time-Periodic Modelling of Single-Phase Elementary Phase-Locked-Loop

Ratik Mittal
Department of Electrical Engineering
University of South Florida
Tampa, FL 33620, USA
ratik@usf.edu

Zhixin Miao
Department of Electrical Engineering
University of South Florida
Tampa, FL 33620, USA
zmiao@usf.edu

***Abstract*—Phase-locked-loops (PLLs) are the most common synchronization units used for integration of voltage source converters to the power grid. One of such type of PLL is a single phase elementary PLL which is inherently nonlinear. The standard approach of Linear Time Invariant (LTI) modelling generally ignores this nonlinear behaviour. So, to accurately model the PLL with nonlinearity included, Linear Time Periodic (LTP) framework is adopted. In this paper, first the method of extracting LTP model of a single phase elementary PLL is illustrated, then the LTI model is developed from the LTP model by expanding the time periodic quantities into complex Fourier series. The two models obtained are simulated in MATLAB / Simulink. Bode plots are also used to obtain the output variable. The results obtained are subsequently validated with the nonlinear PLL model.**

***Index Terms*—Harmonic analysis, harmonic transfer function, linear time invariant (LTI) systems, linear time periodic (LTP) systems, phase-locked-loop (PLL), power electronics, single phase systems, voltage source converters**

I. Introduction

Power electronics based distributed energy resources (DERs) have gained a tremendous popularity for alternative source of power generation and delivery. Stability issues have been observed for inverter-based resource grid integration [1], [2], [3]. Traditionally, modelling of such power electronics based converters [4], is generally done with the help of LTI approach, which usually ignores high-order harmonics while preserving only the fundamental components. Hence, a precise harmonic analysis is required to the system with high-order harmonics included.

To accurately capture these higher order harmonics for steady state analysis, LTP based modelling framework is quite useful. LTP based modelling was introduced by Werely [5], with an objective of analysing time periodic systems, by mapping the LTP model to a LTI model. With, the introduction of harmonics of the state variables, LTP model provided an accurate picture of the nonlinear system. Same approach is used in [6], [7], [8] to obtain the harmonic state space model of power electronics based converters.

One of the key elements of grid connected power converters is PLLs, which enables the efficient and reliable integration of power converters to the grid. One such kind of PLL is the single phase elementary PLL and is widely used in the integration of single phase converters to the grid. The aforementioned PLL suffers from the problem of double frequency [9], [10]. This double frequency is of particular interest and not captured for analysis using the traditional LTI modelling [11], [12].

The objective of this paper is:

1) To illustrate the procedure to derive of LTP model of single phase elementary PLL.
2) To map the obtained the LTP model to LTI model.
3) To validate the two models obtained with the nonlinear model of the PLL.

The rest of the paper is organised as follows. Section II and Section III are a brief introduction of single phase elementary PLL and Harmonic State Space modelling respectively. Section IV illustrates the LTP modelling of the PLL. Section V establishes the LTI Model of the PLL. Section VI demonstrates the simulation results for the two models obtained and their validation with nonlinear model of the PLL, in MATLAB/Simulink. Section VII concludes the paper.

II. Single Phase Elementary PLL

PLLs are the most common synchronization units used for integration of voltage source converters to the power grid. The major objective of this unit is to synchronize the converter with the grid. In this paper, an elementary single phase PLL

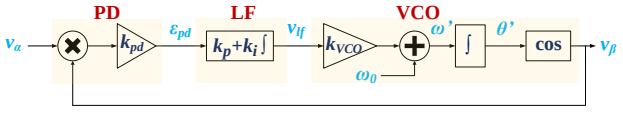

Fig. 1: Block diagram of single phase elementary PLL.

is presented and its models will be investigated [13].
The basic block diagram representation of an elementary PLL is shown in Fig. 1, where the three fundamental parts of any typical PLL (*a*) Phase Detector (PD), (*b*) Loop Filter (LF), and (*c*) Voltage Controlled Oscillator (VCO) are also highlighted.

For analysis, the input applied to the PLL is adopted as:

$$v_\alpha(t) = \hat{V}\sin(\omega_0\, t) \tag{1}$$

where, ω_0 is the fundamental frequency in rad/s, and $\hat{V}$ is the peak magnitude of the input voltage signal.

III. Review of Harmonic State Space Model

In this section the concept of Harmonic State Space (HSS) modelling as discussed in [5] is outlined. On the same lines as the LTI system, the LTP system's dynamic equations can be represented as:

$$\dot{x(t)} = A(t)\,x(t) + B(t)\,u(t) \tag{2}$$

$$y(t) = C(t)\,x(t) + D(t)\,u(t) \tag{3}$$

where, $A(t)$, $B(t)$, $C(t)$ and $D(t)$ are time-periodic matrices. For dynamic analysis of such systems, harmonic balance method [14] is used, which refers to the series expansion of the periodic parts of the solution as complex Fourier series. Now, we can assume general format of $x(t)$ as an exponentially modulated periodic signal:

$$x(t) = \sum_{n=-\infty}^{\infty} X_n\, e^{st}\, e^{j\,n\,\omega_0\,t} \tag{4}$$

where, s is a complex number, and X_n is the complex Fourier's coefficient, which is time invariant in nature. In a similar way $y(t)$ and $u(t)$ are defined. The dynamic matrix in (2)-(3) can be expanded in a complex Fourier series,

$$A(t) = \sum_{m=-\infty}^{\infty} A_m\, e^{j\,m\,\omega_0\,t} \tag{5}$$

and similarly for $B(t)$, $C(t)$ and $D(t)$.
Using (4)-(5), in (2) and (3), the LTP state space model can be mapped to a LTI system as:

$$(s + jn\omega_0)X_n = \sum_{m=-\infty}^{\infty} A_{n-m}X_m + \sum_{m=-\infty}^{\infty} B_{n-m}U_m \tag{6}$$

$$Y_n = \sum_{m=-\infty}^{\infty} C_{n-m}X_m + \sum_{m=-\infty}^{\infty} D_{n-m}U_m \tag{7}$$

Further simplification of (6) and (7) can be done as:

$$s\boldsymbol{X} = (\boldsymbol{A} - \boldsymbol{N})\,\boldsymbol{X} + \boldsymbol{B}\,\boldsymbol{U} \tag{8}$$

$$\boldsymbol{Y} = \boldsymbol{C}\,\boldsymbol{X} + \boldsymbol{D}\,\boldsymbol{U} \tag{9}$$

where, $\boldsymbol{A}$, $\boldsymbol{B}$, $\boldsymbol{C}$, and $\boldsymbol{D}$ are the Toeplitz matrices of the Fourier coefficient of time periodic $A(t)$, $B(t)$, $C(t)$ and $D(t)$ respectively and $\boldsymbol{N}$ represents a diagonal matrix that contains the information about the various frequencies.

A. Harmonic Transfer Function

Equations (8) and (9) are also used to determine the Harmonic Transfer Function" for the system represented by (2) and (3). The "Harmonic Transfer Function" (**HTF**), which is represented as $\boldsymbol{G(s)}$ is an infinite dimensional matrix of Fourier coefficients, that describes the harmonic input-output relationship [5].
HTF can be expressed as:

$$\boldsymbol{G(s)} = \boldsymbol{C}\,[\boldsymbol{s}\,\boldsymbol{I} - \boldsymbol{A} + \boldsymbol{N}]^{-1}\,\boldsymbol{B} + \boldsymbol{D} \tag{10}$$

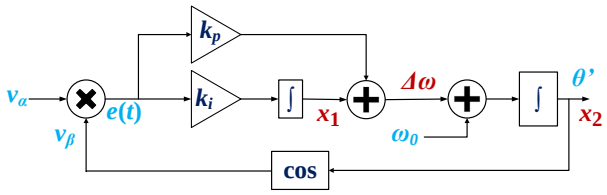

Fig. 2: Block diagram of single phase elementary PLL, adopted for LTP modelling.

IV. LTP Modelling

For obtaining the LTP model of the single phase elementary PLL, the block diagram as shown in Fig. 2 is adopted, and the input signal to the PLL is given as:

$$v_\alpha(t) = \hat{V}\sin(\omega_0\,t\,+\,\Delta\,\theta) \tag{11}$$

where, $\Delta\,\theta$ represents small perturbation in the input signal. States x_1 and x_2 are notated in Fig. 2. The output signal generated is represented as:

$$v_\beta(t) = \hat{V}'\cos(\omega_0\,t\,+\,\Delta\,\theta') \tag{12}$$

where, $\Delta\,\theta'$ represents small deviation in the output signal due to perturbation in the input and $\hat{V}'$ is the estimated peak magnitude of the output voltage signal.
The phase error signal can be expressed as:

$$e(t) = v_\alpha(t) \times v_\beta(t) \tag{13}$$

$$e(t) = (\hat{V}\sin(\omega_0\,t\,+\,\Delta\,\theta)) \times \hat{V}'\cos(\omega_0\,t\,+\,\Delta\,\theta')$$

$$e(t) = \frac{\hat{V}\,\hat{V}'}{2}[\sin(2\,\omega_0\,t + \Delta\,\theta + \Delta\,\theta') + \sin(\Delta\,\theta + \Delta\,\theta')] \tag{14}$$

Assuming the perturbations to be small, (14) can be expressed in terms of Taylor's series as,

$$e(t) \approx \frac{\hat{V}\,\hat{V}'}{2}[\sin(2\,\omega_0\,t) + \cos(2\,\omega_0\,t)\,(\Delta\,\theta + \Delta\,\theta') + (\Delta\,\theta - \Delta\,\theta')]$$

$$e(t) \approx \frac{\hat{V}\,\hat{V}'}{2}[\sin(2\,\omega_0\,t) + (\cos(2\,\omega_0\,t) + 1)\,(\Delta\,\theta) + (\cos(2\,\omega_0\,t) - 1)\,(\Delta\,\theta')] \tag{15}$$

The differential equations for states x_1 and x_2 (Fig. 2) can be expressed as:

$$\dot{x_1}(t) = k_i\,e(t) \tag{16}$$

$$\dot{x_2}(t) = x_1 + k_p\,e(t) \tag{17}$$

k_p and k_i are proportional and integral gain of the PI controller respectively. For simplicity, assuming $\hat{V} \approx \hat{V}'$.
Using (15), (16) and (17) becomes:

$$\begin{aligned} \dot{x_1}(t) = k_i \frac{\hat{V}}{2} [\cos(2\,\omega_0\,t) - 1]\, x_2 + \\ k_i \frac{V}{2} [\cos(2\,\omega_0\,t) + 1]\, u + k_i \frac{\hat{V}}{2} [\sin(2\,\omega_0\,t)] \end{aligned} \tag{18}$$

$$\begin{aligned} \dot{x_2}(t) = x_2 + k_p \frac{\hat{V}}{2} [\cos(2\omega_0\,t) - 1]\, x_2 + \\ k_p \frac{V}{2} [\cos(2\omega_0\,t) + 1]\, u + k_i \frac{\hat{V}}{2} [\sin(2\omega_0\,t)] \end{aligned} \tag{19}$$

A. Output variable

To complete the state space modelling, output variable (y) is selected as $\Delta\omega$, which is the small deviation of the frequency (in rad/s) from the operating frequency of ω_0. Again, referring to Fig. 2, output variable can be expressed as:

$$y(t) = x_1 + k_p\, e(t) \tag{20}$$

Using (15), (20) can be transformed as:

$$\begin{aligned} y(t) = x_1 + k_p \frac{\hat{V}}{2} [\cos(2\,\omega_0\,t) - 1]\, x_2 + \\ k_p \frac{V}{2} [\cos(2\,\omega_0\,t) + 1]\, u + k_p \frac{\hat{V}}{2} [\sin(2\,\omega_0\,t)] \end{aligned} \tag{21}$$

B. State Space Equations

From (18), (19) and (21), the state space equations can be formulated as:

$$\begin{aligned} \begin{bmatrix} \dot{x_1} \\ \dot{x_2} \end{bmatrix} = \overbrace{\begin{bmatrix} 0 & k_i \frac{\hat{V}}{2} [\cos(2\,\omega_0\,t) - 1] \\ 1 & k_p \frac{\hat{V}}{2} [\cos(2\omega_0\,t) - 1] \end{bmatrix}}^{A(t)} \overbrace{\begin{bmatrix} x_1 \\ x_2 \end{bmatrix}}^{x(t)} + \\ \overbrace{\frac{\hat{V}}{2} [\cos(2\,\omega_0\,t) + 1] \begin{bmatrix} k_p \\ k_i \end{bmatrix}}^{B(t)} u + \\ \overbrace{\frac{\hat{V}}{2} [\sin(2\,\omega_0\,t)] \begin{bmatrix} k_p \\ k_i \end{bmatrix}}^{r_1(t)} \end{aligned} \tag{22}$$

$$\begin{aligned} y(t) = \overbrace{\begin{bmatrix} 1 & k_p \frac{\hat{V}}{2} (\cos(2\,\omega_0) - 1) \end{bmatrix}}^{C(t)} + \\ \overbrace{k_p [\frac{\hat{V}}{2} (\cos(2\,\omega_0) + 1)]}^{D(t)} + \overbrace{k_p \frac{\hat{V}}{2} [\sin(2\,\omega_0\,t)]}^{r_2(t)} \end{aligned} \tag{23}$$

From (22)-(23), it is noticeable that matrices $A(t)$, $B(t)$, $C(t)$ and $D(t)$ are time-periodic with a period of $T/2$, where T ($= 2\pi/\omega_0$) is the fundamental time period. The matrix $r_1(t)$ and $r_2(t)$ are the noise matrix. Therefore, (22) and (23) represents the complete LTP model of an elementary single phase PLL.

V. LTI Modelling

As outlined in section III, for extracting LTI model promptly from the LTP model expressed in (22) and (23), the periodic terms are expanded using complex Fourier coefficients. For analysis in this paper, state variables are assumed to have three frequency components i.e. 0 Hz, and $\pm$ 120 Hz, while input ($\Delta\,\theta$) is just a DC variable, and are represented in (24) and (25) respectively.

$$x(t) = X_0 + X_2\, e^{j\,2\,\omega_0\,t} + X_{-2}\, e^{-j\,2\,\omega_0\,t} \tag{24}$$

$$u(t) = U_0 \tag{25}$$

where X_0 and $X_{\pm 2}$ are the time invariant complex Fourier coefficients of $x(t)$. Relating (24) and (25) to (4), the expression of $x(t)$ and $u(t)$ can further be written as:

$$\begin{aligned} e^{s\,t} x(t) = X_0\, e^{s\,t} + X_2\, e^{(s+j\,2\,\omega_0)\,t} + X_{-2}\, e^{(s-j\,2\,\omega_0)t} \\ e^{s\,t} u(t) = U_0\, e^{s\,t} \end{aligned} \tag{26}$$

Similarly, the time periodic terms, $y(t)$ is expressed.

A. LTI System Formation

Using (26) in (2) and (3), the LTI system is formed as follows:

$$\begin{aligned} s\,X_0 &= (A_0\,X_0 + A_2\,X_{-2} + A_{-2}\,X_2) + B_0\,U_0 + R_{1,(0)} \\ (s + j2\,\omega_0)\,X_2 &= (A_0\,X_2 + A_2\,X_0) + B_2\,U_0 + R_{1,(2)} \\ (s - j2\,\omega_0)\,X_{-2} &= (A_0\,X_{-2} + A_{-2}\,X_0) + B_{-2}\,U_0 + R_{1,(-2)} \end{aligned} \tag{27}$$

Similarly, output variable y can be defined as:

$$\begin{aligned} Y_0 &= (C_0\,X_0 + C_2\,X_{-2} + C_{-2}\,X_2) + D_0\,U_0 + R_{2,(0)} \\ Y_2 &= (C_0\,X_2 + C_2\,X_0) + D_2\,U_0 + R_{2,(2)} \\ Y_{-2} &= (C_0\,X_{-2} + C_{-2}\,X_0) + C_{-2}\,U_0 + R_{2,(-2)} \end{aligned} \tag{28}$$

Re-arranging (27) and (28) in matrix format:

$$\begin{aligned} s \begin{bmatrix} X_{-2} \\ X_0 \\ X_2 \end{bmatrix} = \left(\overbrace{\begin{bmatrix} A_0 & A_{-2} & 0 \\ A_2 & A_0 & A_{-2} \\ 0 & A_2 & A_0 \end{bmatrix}}^{\mathbf{A}} - \overbrace{\begin{bmatrix} -2j\omega_0 & & \\ & 0 & \\ & & 2j\omega_0 \end{bmatrix}}^{\mathbf{N}} \right) \times \\ \begin{bmatrix} X_{-2} \\ X_0 \\ X_2 \end{bmatrix} + \overbrace{\begin{bmatrix} B_{-2} \\ B_0 \\ B_2 \end{bmatrix}}^{\mathbf{B}} U_0 + \overbrace{\begin{bmatrix} R_{1,(-2)} \\ R_{1,(0)} \\ R_{1,(2)} \end{bmatrix}}^{R_1} \end{aligned} \tag{29}$$

$$\begin{aligned} \begin{bmatrix} Y_{-2} \\ Y_0 \\ Y_2 \end{bmatrix} = \Big(\overbrace{\begin{bmatrix} C_0 & C_{-2} & 0 \\ C_2 & C_0 & C_{-2} \\ 0 & C_2 & C_0 \end{bmatrix}}^{\mathbf{C}} \Big) \begin{bmatrix} X_{-2} \\ X_0 \\ X_2 \end{bmatrix} + \\ \overbrace{\begin{bmatrix} D_{-2} \\ D_0 \\ D_2 \end{bmatrix}}^{\mathbf{D}} U_0 + \overbrace{\begin{bmatrix} R_{2,(-2)} \\ R_{2,(0)} \\ R_{2,(2)} \end{bmatrix}}^{R_2} \end{aligned} \tag{30}$$

In (29) and (30), $\boldsymbol{A}$, $\boldsymbol{B}$, $\boldsymbol{C}$, $\boldsymbol{D}$, $\boldsymbol{R_1}$ and $\boldsymbol{R_2}$ are Toeplitz matrices, as described in Section III. Therefore, (29) and

$$B_0 = \frac{\hat{V}}{2}\begin{bmatrix} k_i \\ k_p \end{bmatrix},\ B_2 = B_{-2} = \frac{\hat{V}}{4}\begin{bmatrix} k_i \\ k_p \end{bmatrix} \quad C_0 = \begin{bmatrix} 1 & -k_p\frac{\hat{V}}{2} \end{bmatrix},\ C_2 = C_{-2} = \begin{bmatrix} 1 & k_p\frac{\hat{V}}{4} \end{bmatrix} \quad D_0 = k_p\frac{\hat{V}}{2},\ D_2 = D_{-2} = k_p\frac{\hat{V}}{4} \tag{33}$$

$$R_{1,(0)} = 0,\ R_{1,(2)} = \frac{\hat{V}}{4\,j}\begin{bmatrix} k_i \\ k_p \end{bmatrix},\ R_{1,(-2)} = -\frac{\hat{V}}{4\,j}\begin{bmatrix} k_i \\ k_p \end{bmatrix} \quad R_{2,(0)} = 0,\ R_{2,(2)} = k_p\frac{\hat{V}}{4\,j},\ R_{2,(-2)} = -k_p\frac{\hat{V}}{4\,j} \tag{34}$$

(30) completes the mapping of LTP model of single phase elementary PLL to LTI system. From (22), matrix $A(t)$ is a time periodic in nature. In a similar way as (24), $A(t)$ is equal to:

$$A(t) = A_0 + A_2\, e^{j\,2\,\omega_0\,t} + A_{-2}\, e^{-j\,2\,\omega_0\,t} \tag{31}$$

where, A_0, A_2 andA_{-2} are complex Fourier coefficients at 0 Hz and $\pm$120 Hz respectively. Now, to extract these terms, $A(t)$ is expressed as:

$$A(t) = \overbrace{\begin{bmatrix} 0 & -k_i\frac{\hat{V}}{2} \\ 1 & -k_p\frac{\hat{V}}{2} \end{bmatrix}}^{A_0} + \overbrace{\frac{1}{2}\begin{bmatrix} 0 & k_i\frac{\hat{V}}{2} \\ 0 & k_p\frac{\hat{V}}{2} \end{bmatrix}}^{A_2} e^{j\,2\,\omega_0\,t} + \overbrace{\frac{1}{2}\begin{bmatrix} 0 & k_i\frac{\hat{V}}{2} \\ 0 & k_p\frac{\hat{V}}{2} \end{bmatrix}}^{A_{-2}} e^{-j\,2\,\omega_0\,t} \tag{32}$$

In the analogous fashion as provided in (31) and (32), other time periodic dynamic matrices in (22) and (23) can be defined. The Fourier coefficients for $B(t)$, $C(t)$, $D(t)$, $r_1(t)$ and $r_2(t)$ are expressed in (33)-(34) at top of this page.

Note: X_{-2} is a (2 $\times$ 1) column vector, which represents complex Fourier coefficients of x_1 and x_2 at -120 Hz i.e..

$$[X_{-2}] = \begin{bmatrix} X_{1,\,(-2)} \\ X_{2,\,(-2)} \end{bmatrix} \tag{35}$$

In a similar manner, X_0 and X_2 are defined.

$$[X_0] = \begin{bmatrix} X_{1,\,(0)} \\ X_{2,\,(0)} \end{bmatrix},\quad [X_2] = \begin{bmatrix} X_{1,\,(2)} \\ X_{2,\,(2)} \end{bmatrix}$$

VI. Simulation and Results

In this section, state space models obtained previously are simulated using MATLAB / Simulink, and are bench-marked with nonlinear model of single phase elementary PLL (Fig. 2). For nonlinear model, parameters k_{pd} and k_{VCO} are considered as unity. A step change is applied to the input u (= $\Delta\theta$) at t = 0.5s of 10° (Fig. 3). The parameters used in the simulation are listed in Table I.

TABLE I: Parameters used for Simulations

S.No	Parameter	Value
1	$\hat{V}$	1 $p.u$
2	k_p	60
3	k_i	1400
4	f_0	60 Hz

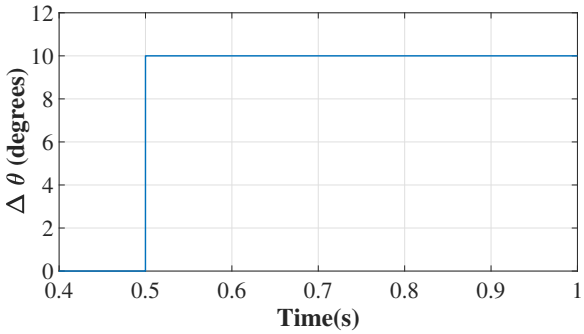

Fig. 3: Step change in the input u = $\Delta\theta$, at t = 0.5 s.

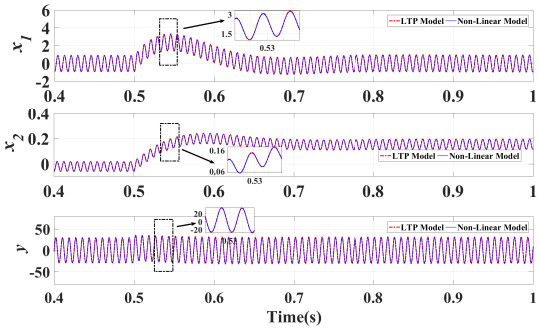

Fig. 4: Performance of LTP Model compared to the nonlinear model, when a phase jump of 10° is introduced.

A. Simulation results from LTP Model

The step response for LTP model and nonlinear model is shown in Fig. 4. It is noticeable from the plots in Fig. 4 that, LTP model and nonlinear model corroborates.

B. Simulation Results from LTI Model

For the LTI model, the states and the output variables are in the form of complex Fourier coefficients. The step change response of the LTI system obtained in Section V, is shown in Fig. 5 and Fig. 6. The plots shown are the absolute value of the complex Fourier coefficients (for 0 Hz and $\pm$120 Hz) for X and Y.

For validation, FFT was performed on states x_1, x_2 and y in the nonlinear model. Using FFT, magnitude and phase angle were extracted for x_1, x_2 and y for 0 Hz and 120 Hz. With the

TABLE II: Comparison of Fourier coefficients between LTI model and nonlinear model at steady state.

Harmonics	Fourier Coefficients	LTI Model	Nonlinear Model
-120 Hz	X_1	$0.488\angle 159.5°$	$0.464\angle 157.8°$
	X_2	$0.021\angle 161.27°$	$0.0199\angle 159.8°$
	Y	$15.806\angle 71.269°$	$15.01\angle 69.55°$
0 Hz	X_1	0	0
	X_2	$0.154\angle 0°$	$0.1546\angle 0°$
	Y	0	0
120 Hz	X_1	$0.488\angle -159.5°$	$0.464\angle -157.8°$
	X_2	$0.021\angle 161.27°$	$0.0199\angle -159.8°$
	Y	$15.806\angle -71.269°$	$15.01\angle -69.55°$

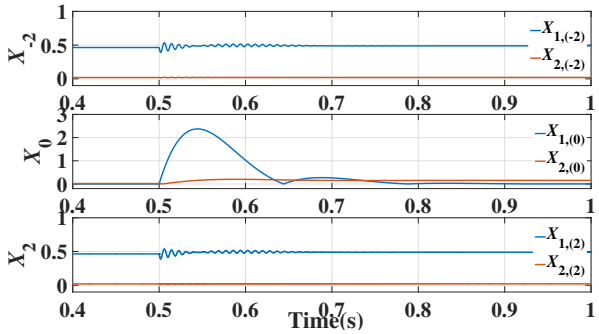

Fig. 5: Absolute value of the complex Fourier coefficients of X.

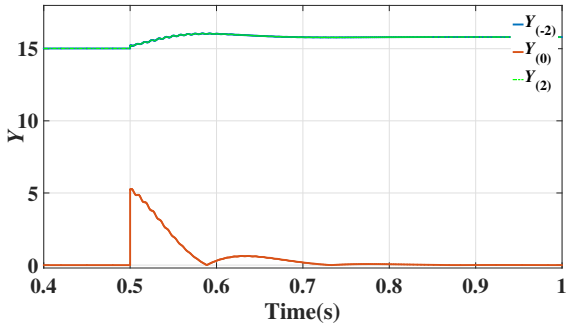

Fig. 6: Absolute value of the complex Fourier coefficients of Y.

help of magnitude and phase angle information, time domain signal is formulated:

$$f(t) = A\,\cos(n\,\omega_0\,t + \alpha) \tag{36}$$

where, A and α are the magnitude and phase obtained from the FFT plots respectively and n is the harmonic order (= 0, 2).

Now, expanding (35) in complex Fourier series format:

$$\begin{aligned} f(t) &= \frac{A}{2}\left(e^{j\,(n\,\omega_0\,t+\alpha)} + e^{-j\,(n\,\omega_0\,t+\alpha)}\right) \\ f(t) &= A\,\overbrace{\left(\frac{e^{j\,\alpha}}{2}\right)}^{F_{(n)}}\,e^{j\,n\omega_0\,t} + A\,\overbrace{\left(\frac{e^{-j\,\alpha}}{2}\right)}^{F_{(-n)}}\,e^{-j\,n\omega_0\,t} \end{aligned} \tag{37}$$

The comparison of Fourier coefficients are listed in Table II. It can be observed from Fig. 6 and Table II, that the Fourier coefficients obtained from LTI model and the nonlinear model verify.

C. *Validation of output Y using Bode Plots*

The state space model presented in (29) and (30), can be used to obtain input-output relationship, as presented below:

$$s\boldsymbol{X} = (\boldsymbol{A} - \boldsymbol{N})\,\boldsymbol{X} + \boldsymbol{B}\,\boldsymbol{U} + \boldsymbol{R_1} \tag{38}$$

$$\boldsymbol{Y} = \boldsymbol{C}\,\boldsymbol{X} + \boldsymbol{D}\,\boldsymbol{U} + \boldsymbol{R_2} \tag{39}$$

From, (38) and using (40) in (39)

$$\boldsymbol{X(s)} = (s\,\boldsymbol{I} - \boldsymbol{A} + \boldsymbol{N})^{-1}(\boldsymbol{B}\,U_0 + \boldsymbol{R_1}) \tag{40}$$

$$\begin{aligned} \boldsymbol{Y(s)} = \overbrace{\left[\boldsymbol{C}\,(s\,\boldsymbol{I} - \boldsymbol{A} + \boldsymbol{N})^{-1}\,\boldsymbol{B} + \boldsymbol{D}\right]}^{\boldsymbol{G(s)}}\,U_0 + \\ \boldsymbol{C}\,(s\,\boldsymbol{I} - \boldsymbol{A} + \boldsymbol{N})^{-1}\,\boldsymbol{R_1} + \boldsymbol{R_2} \end{aligned} \tag{41}$$

From (41), it can be observed that $Y(s)$ has two parts:

$$\boldsymbol{Y_1(s)} = \boldsymbol{G(s)}\,U_0 \tag{42}$$

$$\boldsymbol{Y_2(s)} = \boldsymbol{C}\,(s\,\boldsymbol{I} - \boldsymbol{A} + \boldsymbol{N})^{-1}\,\boldsymbol{R_1} + \boldsymbol{R_2} \tag{43}$$

where, $\boldsymbol{G(s)}$ is the harmonic transfer function. In this section, bode plots for $\boldsymbol{G(s)}$ and $\boldsymbol{Y_2(s)}$ are presented in Fig.9. To validate the results with the non-linear model, $\boldsymbol{Y(s)}$ is extracted using (42) and (43) for a input step change of 10° (i.e. U_0 = 0.1745 radians).

From bode plots of $\boldsymbol{G(s)}$ and $\boldsymbol{Y_2(s)}$ magnitude and phase angle information is obtained at frequency close to 0 Hz. Then the phasor for Y can be formulated as:

$$|Y(j\,\omega)|\angle Y(j\,\omega) = |Y_1(j\,\omega)|\angle Y_1(j\,\omega) + |Y_2(j\,\omega)|\angle Y_2(j\,\omega) \tag{44}$$

for $\omega \to 0$ Hz. The results are listed in Table III. The results obtained from bode plots are compared with complex Fourier coefficients of Y obtained from the non-linear model are presented in Table IV. It can be observed that the results obtained from the non-linear model and frequency domain approach are a close match.

TABLE III: Magnitude and Phase values Y_1, Y_2 and Y at frequency close to 0 Hz

Harmonics	Y_1	Y_2	Y
-120 Hz	$0.527\angle -0.509°$	$14.96\angle 90.6°$	$15.8194\angle 70.58°$
0 Hz	$\approx 0\angle 90°$	$\approx 0\angle -90°$	≈ 0
120 Hz	$0.5.27\angle 0.509°$	$14.96\angle -90.6°$	$15.8194\angle -70.58°$

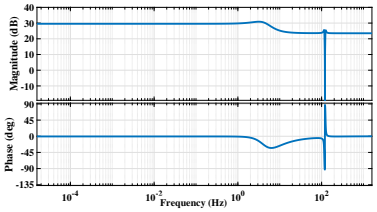

(a) Bode plot of $\boldsymbol{G(s)}$ for -120 Hz component.

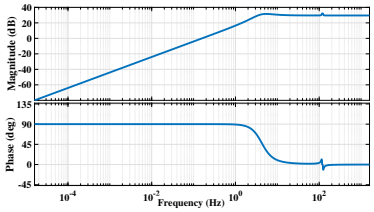

(b) Bode plot of $\boldsymbol{G(s)}$ for 0 Hz component.

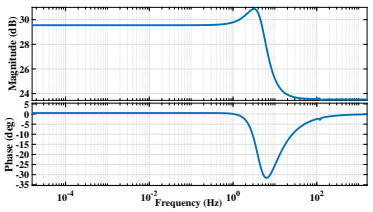

(c) Bode plot of $\boldsymbol{G(s)}$ for 120 Hz component.

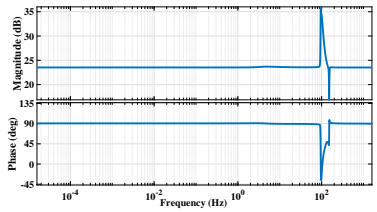

(d) Bode plot of $\boldsymbol{Y_2(s)}$ for -120 Hz component.

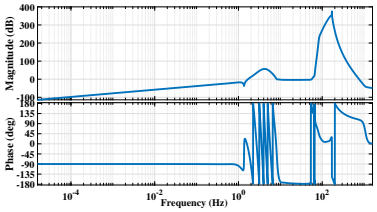

(e) Bode plot of $\boldsymbol{Y_2(s)}$ for 0 Hz component.

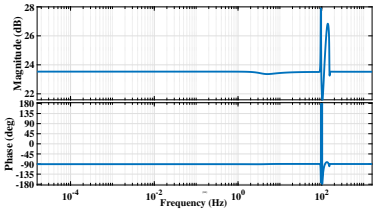

(f) Bode plot of $\boldsymbol{Y_2(s)}$ for 120 Hz component.

Fig. 7: Bode plots for $\boldsymbol{G(s)}$ (harmonic transfer function) and $\boldsymbol{Y_2(s)}$, for 0 and $\pm$120 Hz complex Fourier coefficients.

TABLE IV: Comparison of complex Fourier coefficients of Y obtained from bode plots and nonlinear model

Harmonics	Bode Plots	Non-Linear Model
-120 Hz	$15.8194\angle 70.58°$	$15.01\angle 69.55°$
0 Hz	≈ 0	0
120 Hz	$15.8194\angle -70.58°$	$15.01\angle -69.55°$

VII. Conclusion

This paper illustrated the procedure of deriving of LTP model of single phase elementary PLL. After developing the LTP model, using the concept of complex Fourier series and harmonic balance method, the time varying system was transferred to time in-varying system, so as to develop the LTI model of the PLL. With the LTI model at disposal, the analysis can be done using the conventional LTI techniques. The two models obtained were simulated using MATALB/Simulink, and a phase jump in the input side was also introduced for observing the dynamic response. Bode plots showing input-output relationship are presented in this paper, for extracting the output variable for input step change. The results obtained were validated with the nonlinear model of the PLL.

ACKNOWLEDGEMENT

The authors are grateful to Dr. Lingling Fan of University of South Florida for her guidance and support.

References

[1] L. Xu, L. Fan, and Z. Miao, "Dc impedance-model-based resonance analysis of a vsc–hvdc system," *IEEE Transactions on Power Delivery*, vol. 30, no. 3, pp. 1221–1230, 2015.

[2] L. Wang, X. Xie, Q. Jiang, H. Liu, Y. Li, and H. Liu, "Investigation of ssr in practical dfig-based wind farms connected to a series-compensated power system," *IEEE Transactions on Power Systems*, vol. 30, no. 5, pp. 2772–2779, 2015.

[3] Y. Li, L. Fan, and Z. Miao, "Replicating real-world wind farm ssr events," *IEEE Transactions on Power Delivery*, vol. 35, no. 1, pp. 339–348, 2020.

[4] A. Yazdani and R. Iravani, *Voltage-sourced converters in power systems: modeling, control, and applications*. John Wiley & Sons, 2010.

[5] N. M. Wereley, "Analysis and control of linear periodically time varying systems," Ph.D. dissertation, Massachusetts Institute of Technology, 1990.

[6] J. Kwon, X. Wang, F. Blaabjerg, C. L. Bak, V. Sularea, and C. Busca, "Harmonic interaction analysis in a grid-connected converter using harmonic state-space (hss) modeling," *IEEE Transactions on Power Electronics*, vol. 32, no. 9, pp. 6823–6835, 2017.

[7] C. Zhang, M. Molinas, A. Rygg, J. Lyu, and X. Cai, "Harmonic transfer-function-based impedance modeling of a three-phase vsc for asymmetric ac grid stability analysis," *IEEE Transactions on Power Electronics*, vol. 34, no. 12, pp. 12 552–12 566, 2019.

[8] J. R. C. Orillaza and A. R. Wood, "Harmonic state-space model of a controlled tcr," *IEEE Transactions on Power Delivery*, vol. 28, no. 1, pp. 197–205, 2013.

[9] S. Golestan, M. Monfared, F. D. Freijedo, and J. M. Guerrero, "Design and tuning of a modified power-based pll for single-phase grid-connected power conditioning systems," *IEEE Transactions on Power Electronics*, vol. 27, no. 8, pp. 3639–3650, 2012.

[10] T. Thacker, D. Boroyevich, R. Burgos, and F. Wang, "Phase-locked loop noise reduction via phase detector implementation for single-phase systems," *IEEE Transactions on Industrial Electronics*, vol. 58, no. 6, pp. 2482–2490, 2011.

[11] S. Golestan, J. M. Guerrero, and J. C. Vasquez, "Modeling and stability assessment of single-phase grid synchronization techniques: Linear time-periodic versus linear time-invariant frameworks," *IEEE Transactions on Power Electronics*, vol. 34, no. 1, pp. 20–27, 2019.

[12] S. Golestan, J. Guerrero, J. Vasquez, A. M. Abusorrah, and Y. A. Al-Turki, "Standard sogi-fll and its close variants: Precise ltp modeling and determining stability region/robustness metrics," *IEEE Transactions on Power Electronics*, pp. 1–1, 2020.

[13] R. Teodorescu, M. Liserre, and P. Rodriguez, *Grid converters for photovoltaic and wind power systems*. John Wiley & Sons, 2011, vol. 29.

[14] G. W. Hill *et al.*, "On the part of the motion of the lunar perigee which is a function of the mean motions of the sun and moon," *Acta mathematica*, vol. 8, pp. 1–36, 1886.